Cell Reports Physical Science, Volume *6*

Supplemental information

A battery-free wireless keyboard

Xin Li, Xinyuan Chuai, Yaoyi Li, Yawei Wang, Qitao Lu, Yaozi Zheng, Daxing Zhang, Congsi Wang, Guobiao Hu, and Wei-Hsin Liao

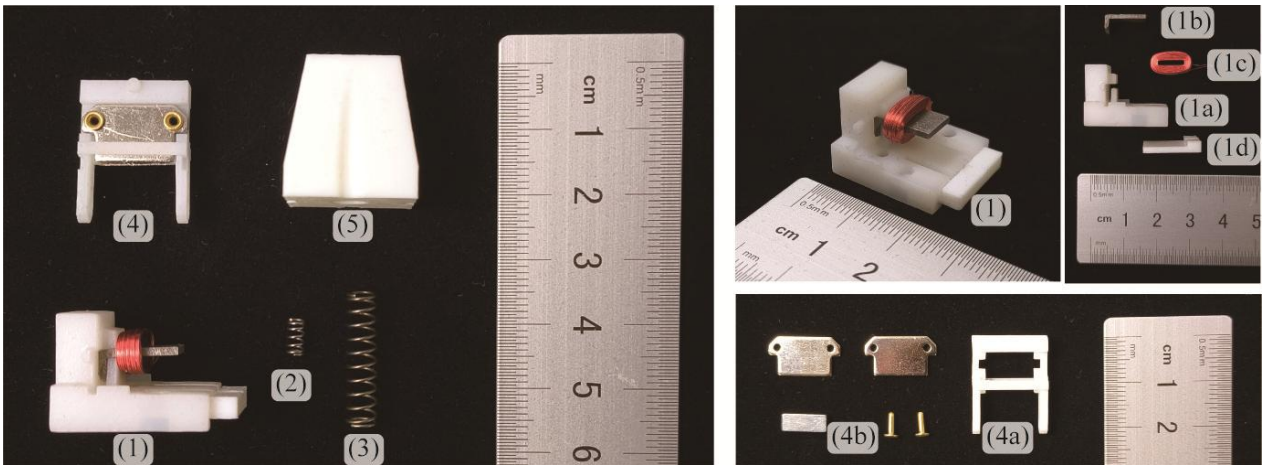

Fig. S1. Detailed disassembly diagram of a single keyboard key.

This figure illustrates the disassembled components of a keyboard key, with certain parts shown from multiple perspectives or in further disassembled states. The components include:

(1) Shell with ferromagnetic core and coil:
- (1a) Shell providing overall support, securing the moving body and ferromagnetic core;
- (1b) Ferromagnetic core;
- (1c) Coil;
- (1d) Shell designed to apply preload to the restoring spring.

(2) Restoring spring.

(3) Buffing spring.

(4) Moving body:
- (4a) Main support structure of the moving body;
- (4b) Magnet and magnetic conductor.

(5) Keycap.

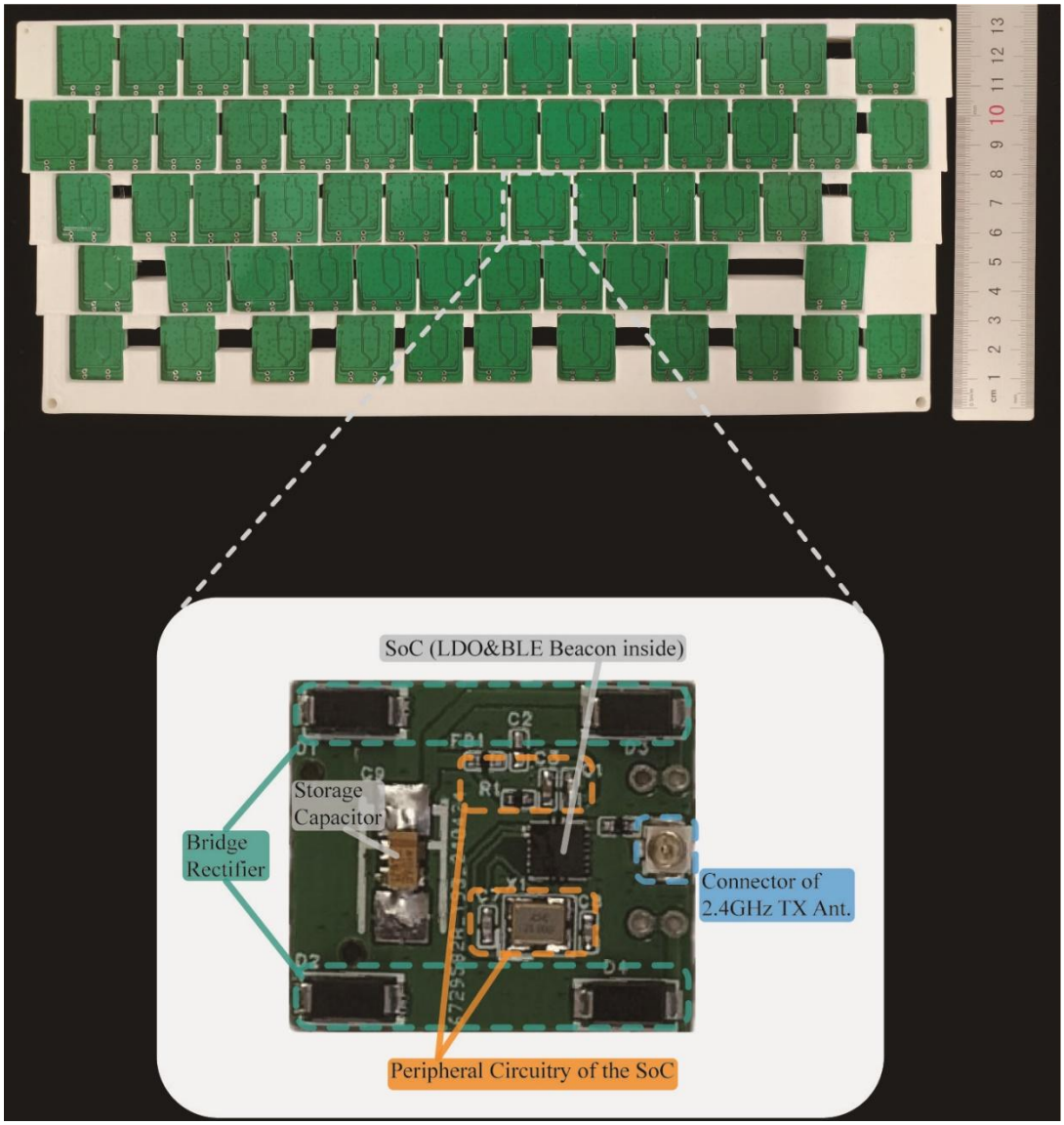

Fig. S2. Circuit layout diagram of the entire keyboard and detailed circuit board embedded beneath a single key.

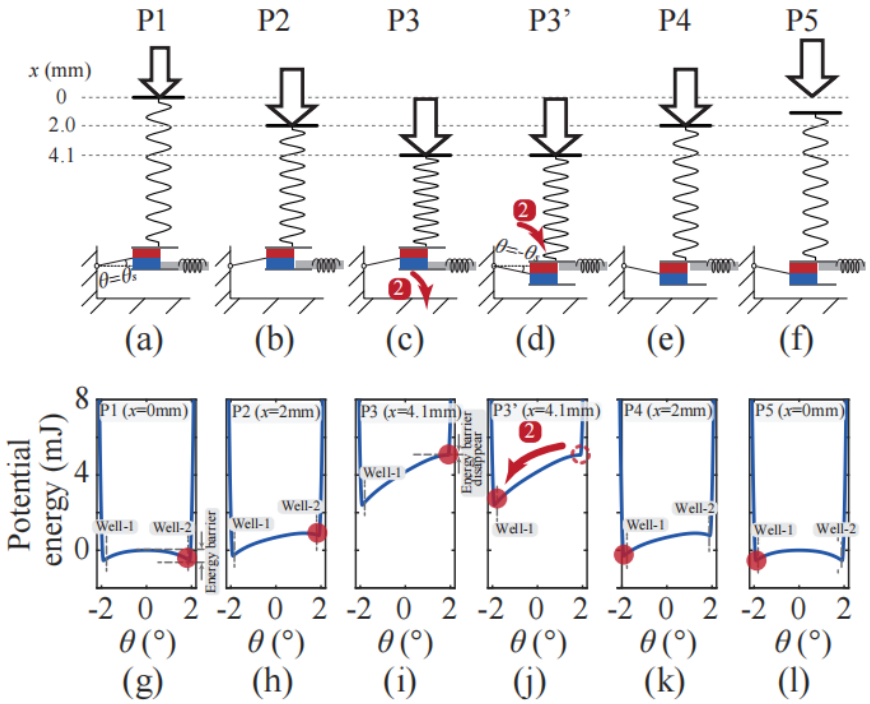

Fig. S3. Energy diagrams for Case #1 with a bistable configuration during a single keystroke motion.

(a)-(f) Potential energy profiles. (g)-(h) Corresponding schematics.
(a) and (g) Starting position with two symmetric wells.
(b) and (h) Intermediate position with two asymmetric wells.
(c) and (i) Operation position at which the energy barrier disappears.
(d) and (j) Operation position at which potential energy is released to this point.
(e) and (k) Restore intermediate position with two wells.
(f) and (l) Restore to the initial position.

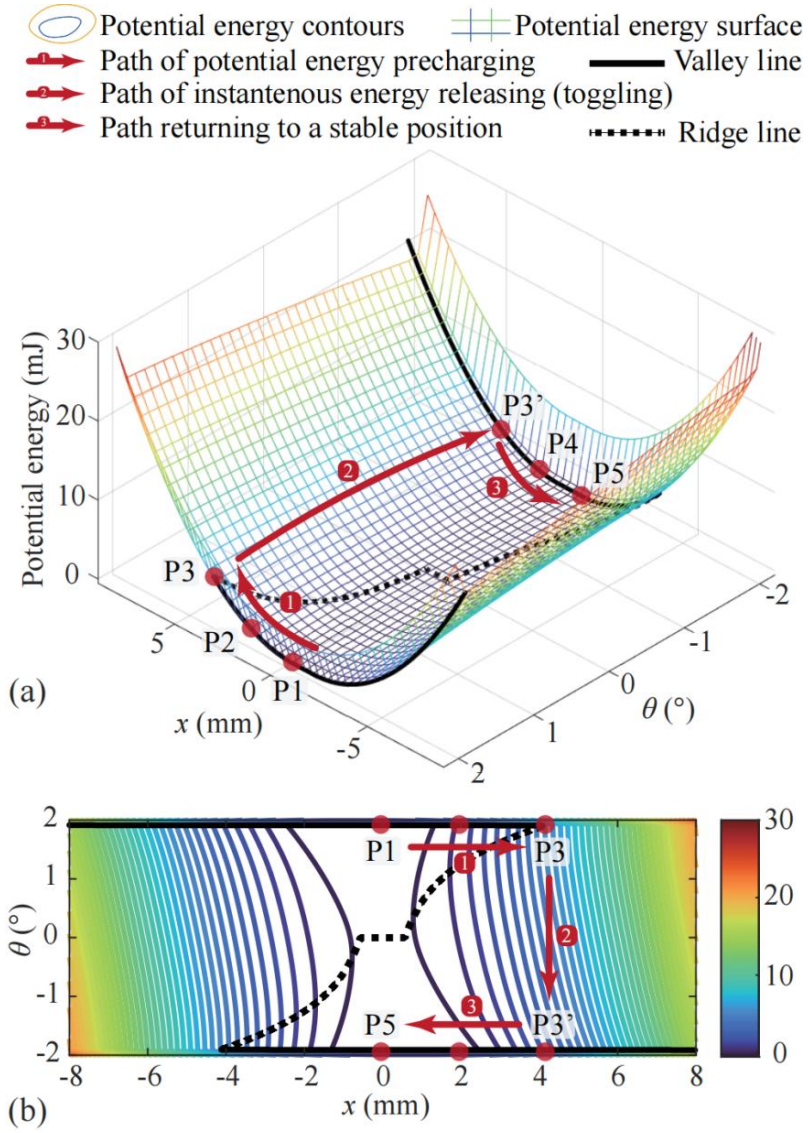

Fig. S4. Potential energy profiles for Case #1 with a bistable configuration during a single keystroke.

(a) 3D contour plot. (b) 2D contour plot.

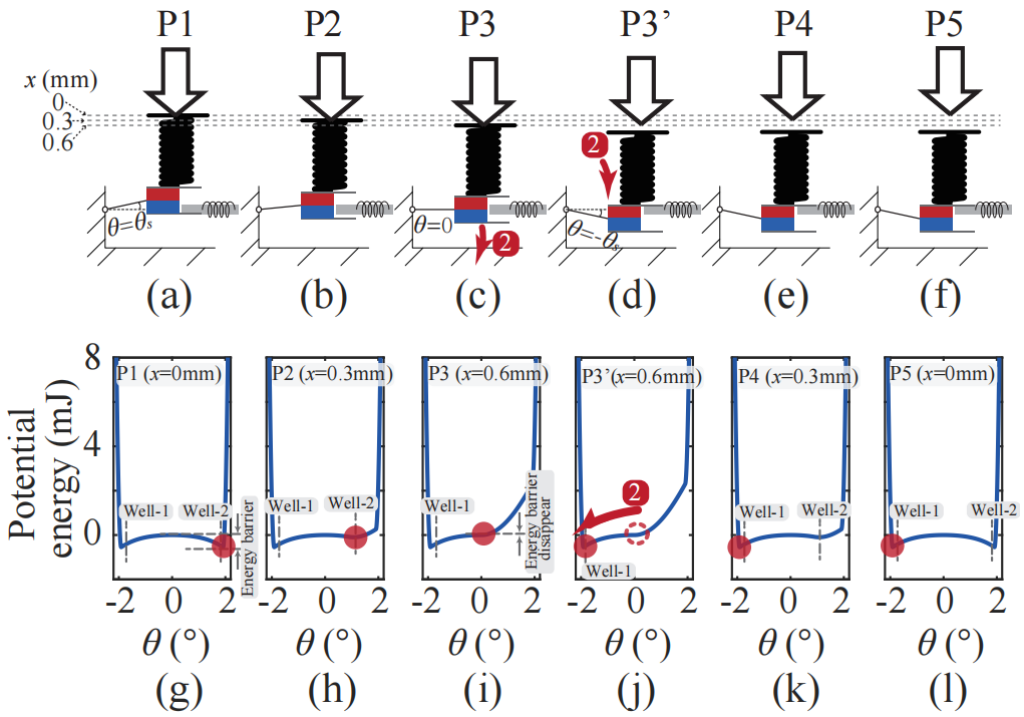

Fig. S5. Energy diagrams for Case #2 under a bistable configuration a with stiff buffering spring.

(a)-(f) Potential energy profiles.
(g)-(l) Corresponding schematics.
(a) and (g) Starting position with two symmetric wells.
(b) and (h) Intermediate position with two asymmetric wells.
(c) and (i) Operation position at which the energy barrier disappears.
(d) and (j) Operation position at which potential energy is released to this point.
(e) and (k) Restore intermediate position with two wells.
(f) and (l) Restore to the initial position.

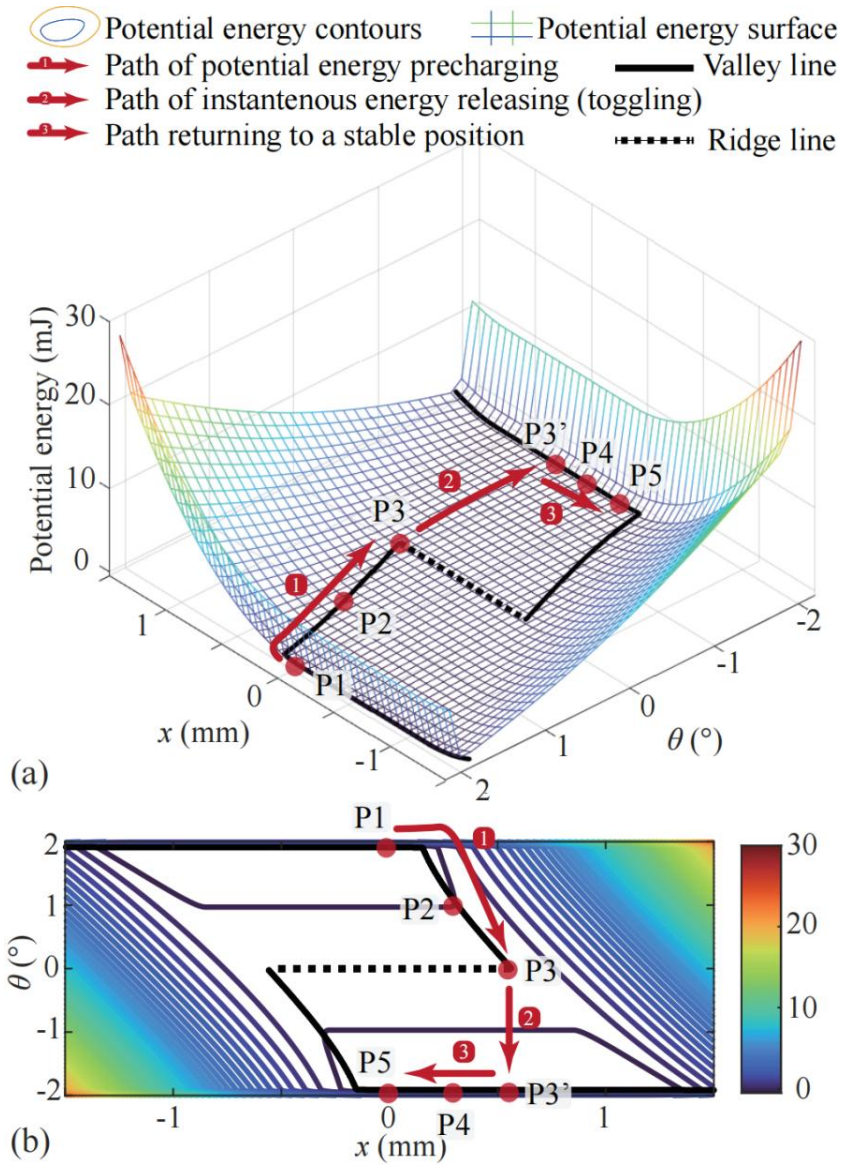

Fig. S6. Potential energy profiles for Case #2 under a bistable configuration and a stiff buffering spring.

(a) 3D contour plot. (b) 2D contour plot.

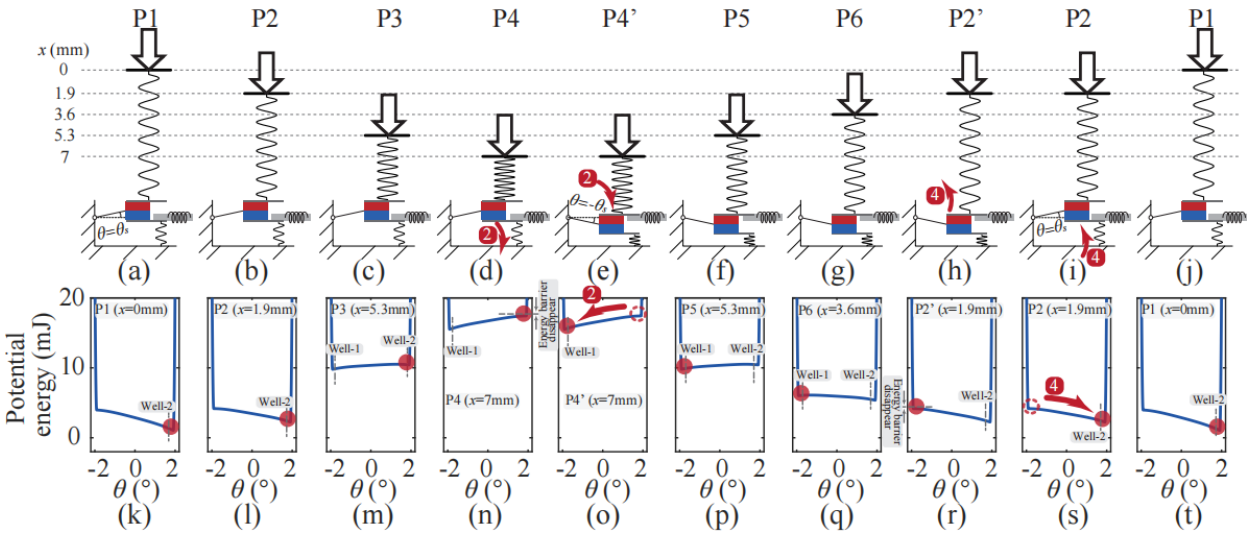

Fig. S7. Energy diagrams for Case #3 with a monostable configuration.

(a) and (k) Starting position with a monostable well.
(b) and (l) Intermediate position with a monstable well.
(c) and (m) Intermediate position with two wells.
(d) and (n) Operation position at which the energy barrier disappears.
(e) and (o) Operation position at which potential energy is released to this point.
(f)-(g) and (p)-(q) Restore intermediate positions with two wells.
(h) and (r) Operation reset position at which the energy barrier disappears again.
(i) and (s) Operation reset position at which potential energy is again released to this point.
(j) and (t) Restore to the initial position.

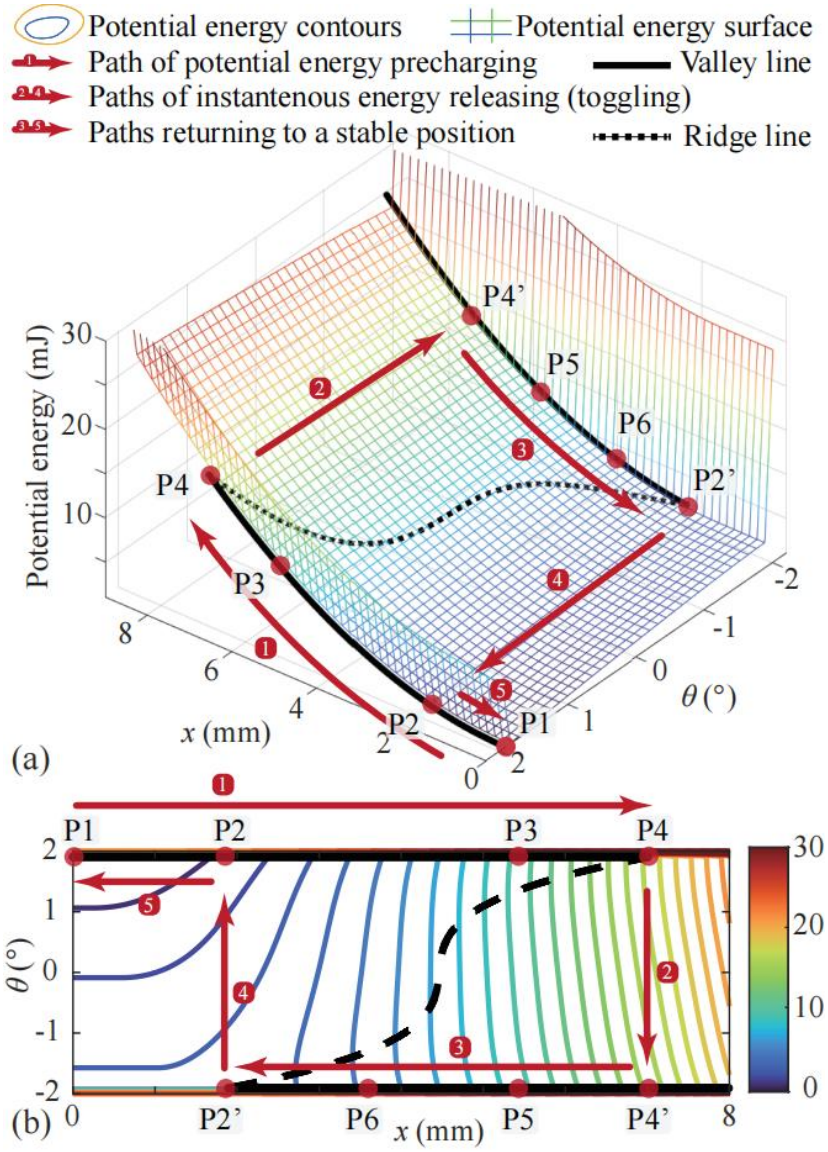

Fig. S8. Potential energy profiles for Case #3 with a monostable configuration.
(a) 3D contour plot. (b) 2D plot.

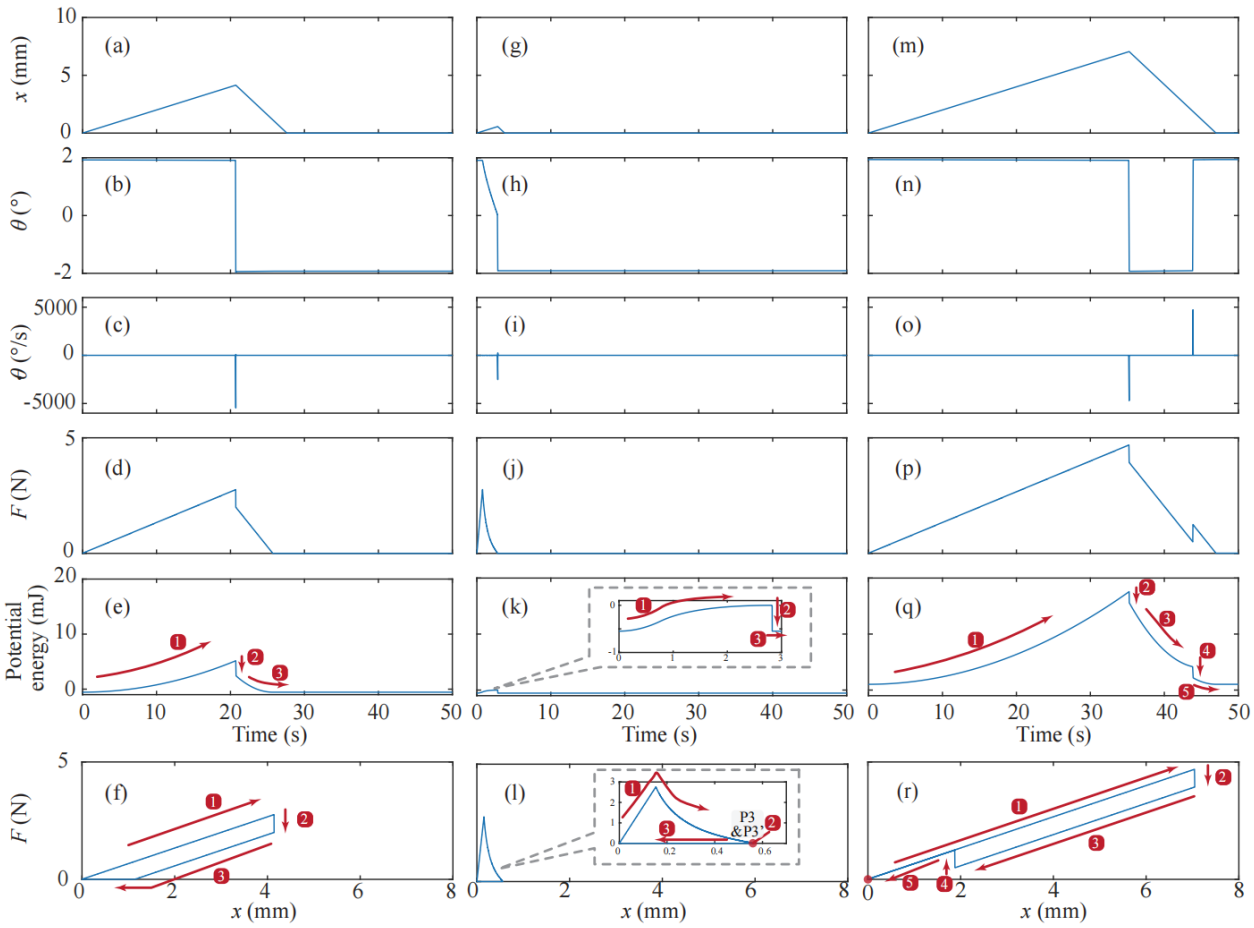

Fig. S9. Simulation results under three cases (Parameters are provided in Table S1).

(a)-(g) Case #1: Bistable configuration with a soft buffering spring.
(f)-(j) Case #2: Bistable configuration with a stiff buffering spring.
(k)-(o) Case #3: Monostable configuration with a restoring spring.

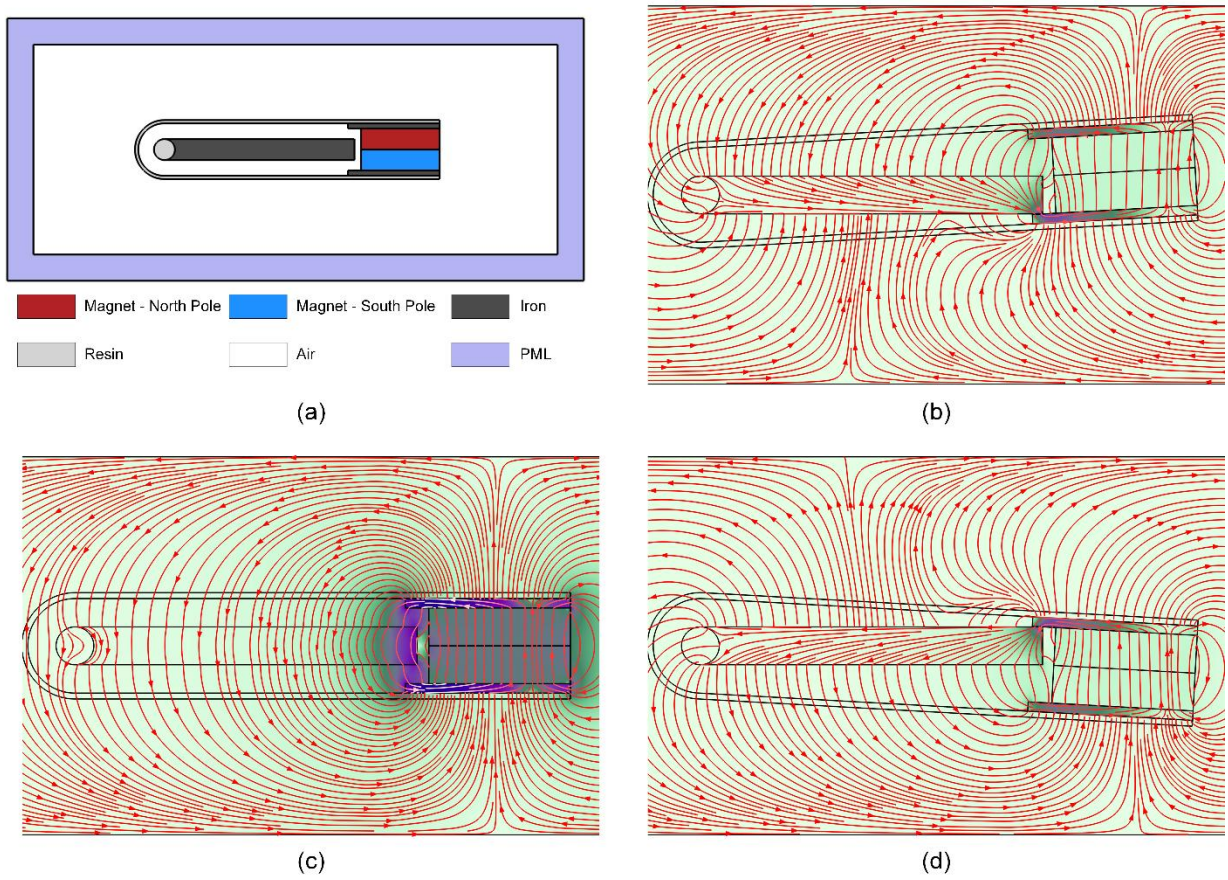

Fig. S10. Finite element simulation of magnetic flux distribution in the pole-swapping process.

(a) COMSOL model showing material regions, including the magnet (north and south poles), iron core, resin, air, and perfectly matched layer (PML).
(b) Magnetic field distribution in the free state (corresponding to P3 in **Fig. 2C**), showing the initial flux direction through the iron core.
(c) Intermediate state during keypress, with the magnet partially displaced.
(d) Fully pressed state (corresponding to P6 in **Fig. 2C**), where the magnet has moved to the bottom position and the magnetic polarity is reversed.
A sudden reversal of magnetic flux direction is clearly observed between (b) and (d), confirming successful pole-swapping and supporting the design principle of flux-driven power generation.

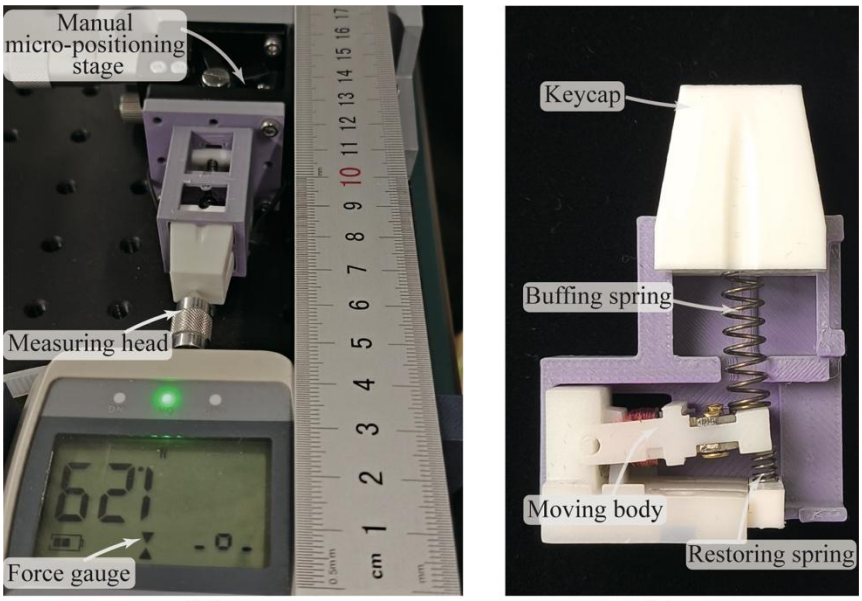

Fig. S11. Pressing force testing setup.
(a) Overview. (b) Single FMH unit (sectional side view).

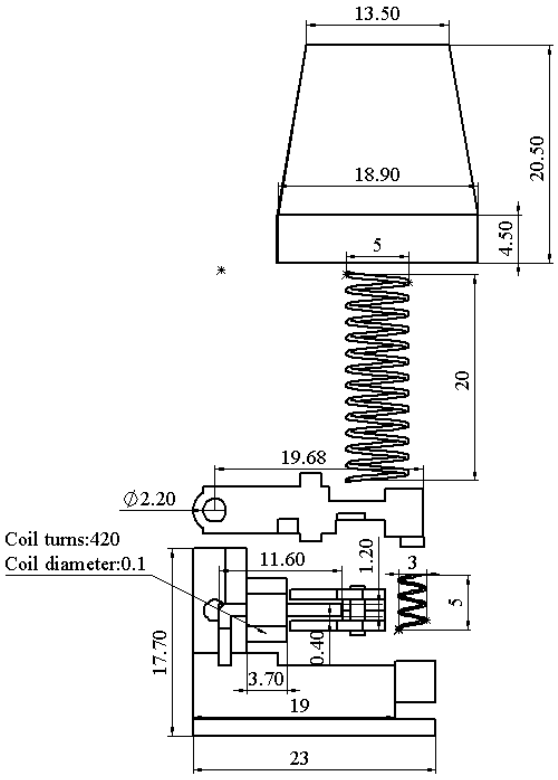

Fig. S12. Mechanical layout and key dimensions of a single FMH.

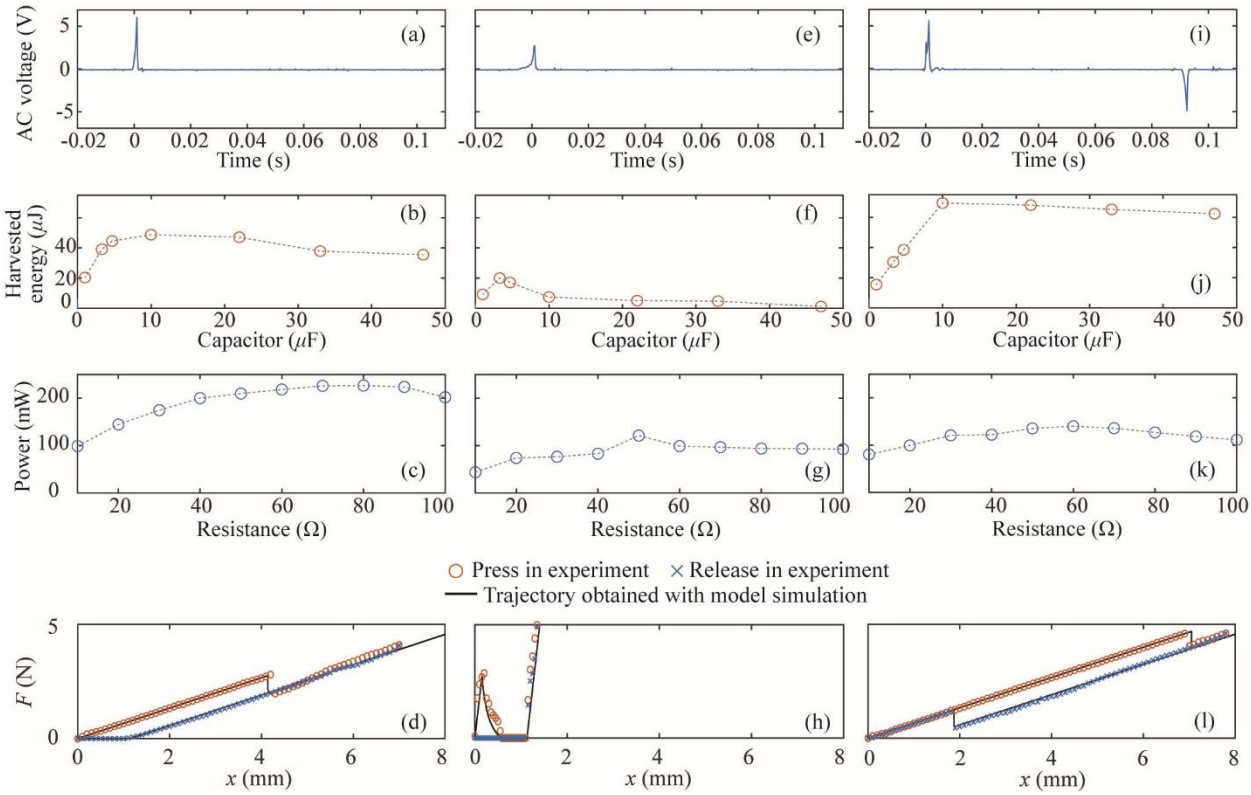

Fig. S13. Test results for the FMH unit during a single keystroke across three cases (Parameters are provided in Table S1 and Table S2).

The first row presents the open-circuit voltage.
The second row shows the harvested energy.
The third row details the maximum instantaneous power of the FMH unit.
The fourth row shows the force-displacement trajectories in experiment and simulation comparison.
(a)-(d) Case 1: Bistable configuration with a soft buffering spring;
(e)-(h) Case 2: Bistable configuration with a stiff buffering spring;
(i)-(l) Case 3: Monostable configuration with a restoring spring.

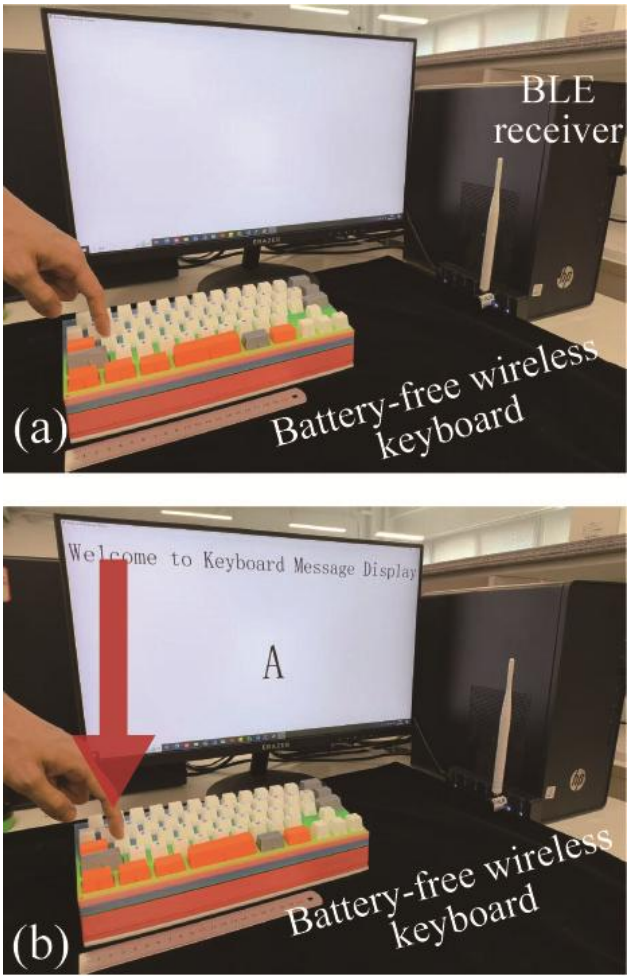

Fig. S14. User interaction with the battery-free wireless keyboard.
(a) Positioning over the key switch ‘A’. (b) Stroke on the key switch ‘A’ and the resultant display.

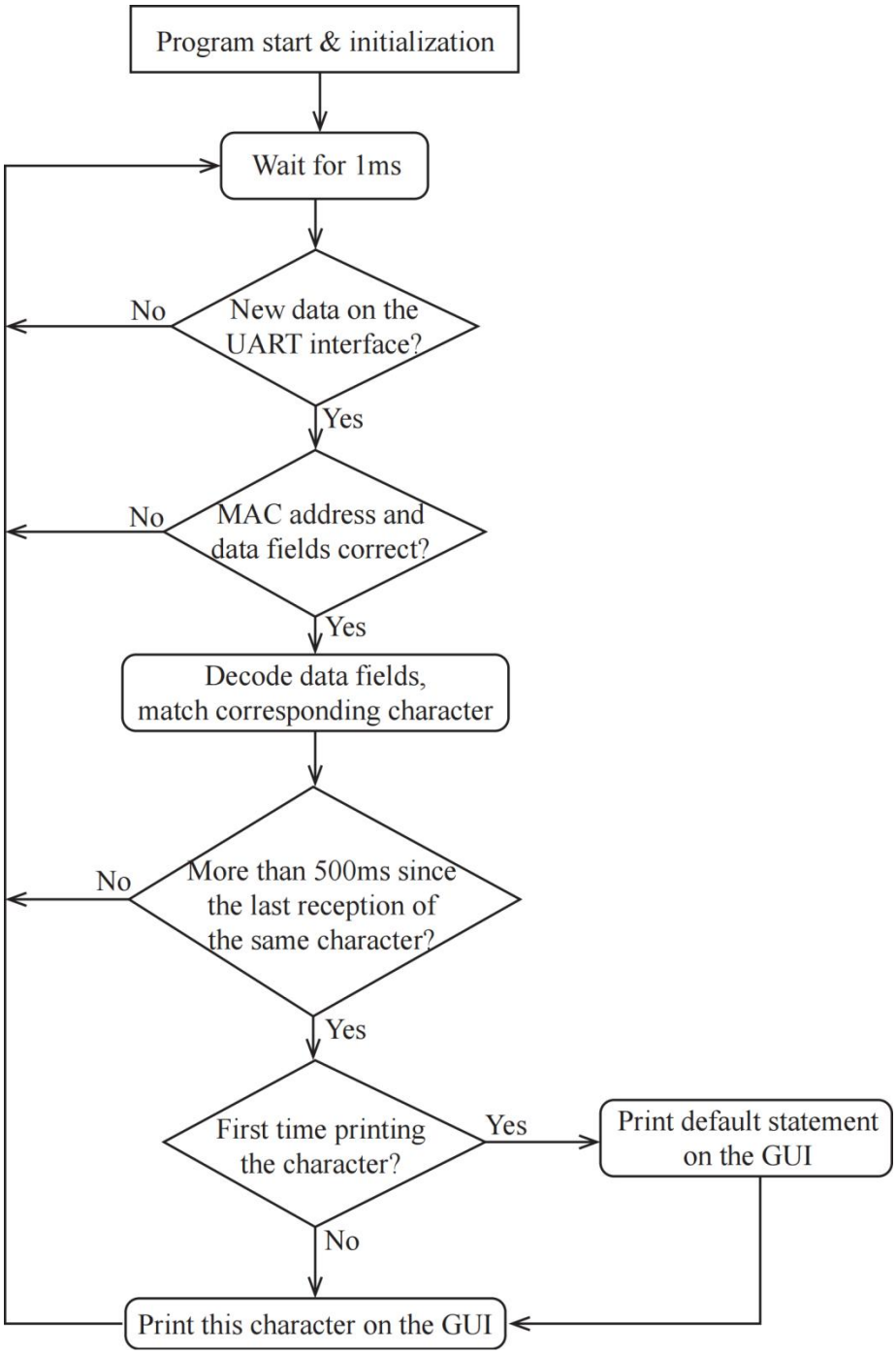

Fig. S15. Flowchart of keypress information processing at the receiver.

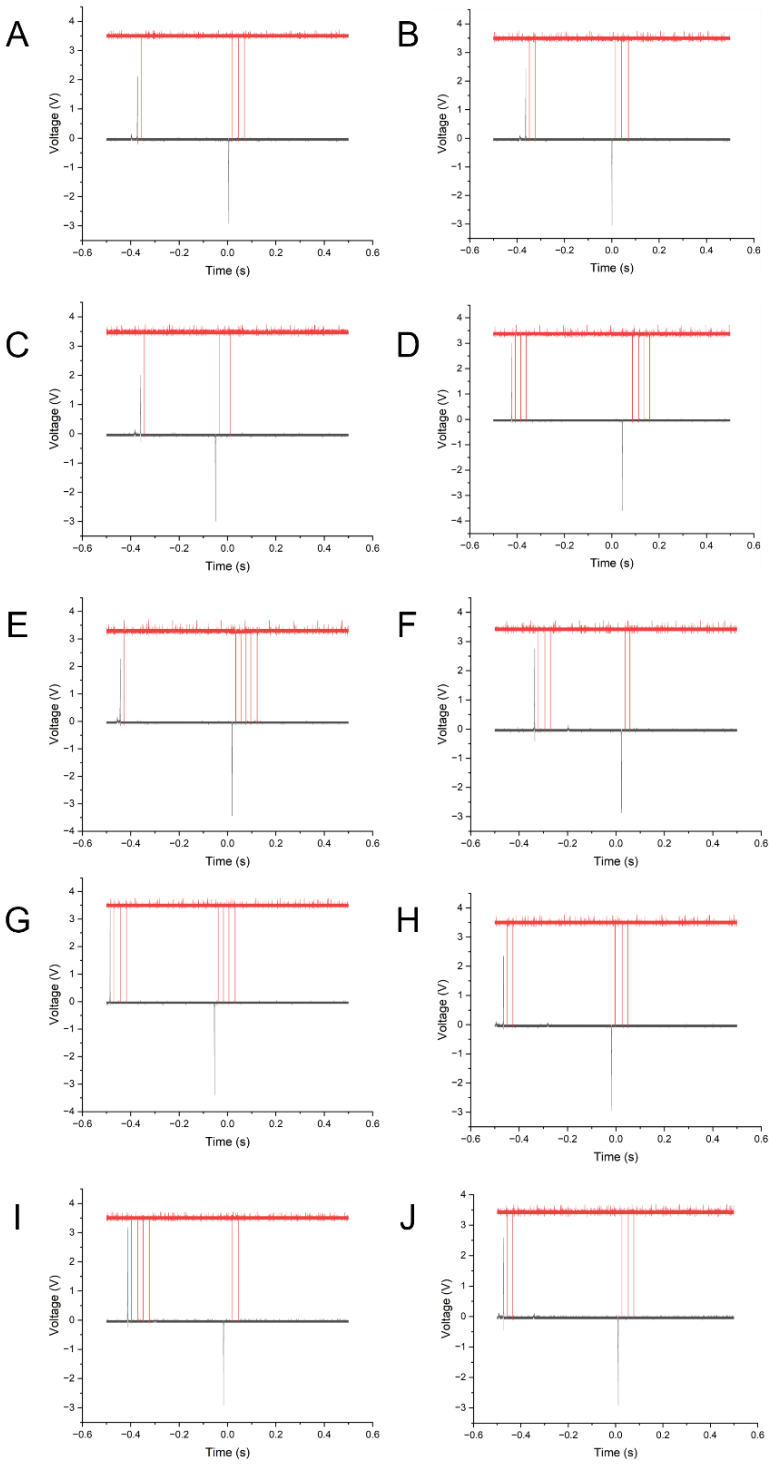

Fig. S16. Raw data for Figure 5C(i).
The black curve represents the voltage output from the FMH (Fingertip Motion Harvester), while the red spikes overlaid on the curve indicate the Bluetooth Low Energy (BLE) signal detection events, as identified by the UART interface.

(A) group 1 test 1. (B) group 2 test 2. (C) group 3 test 3. (D) group 4 test 4. (E) group 5 test 5. (F) group 6 test 6. (G) group 7 test 7. (H) group 8 test 8. (I) group 9 test 9. (J) group 10 test 10.

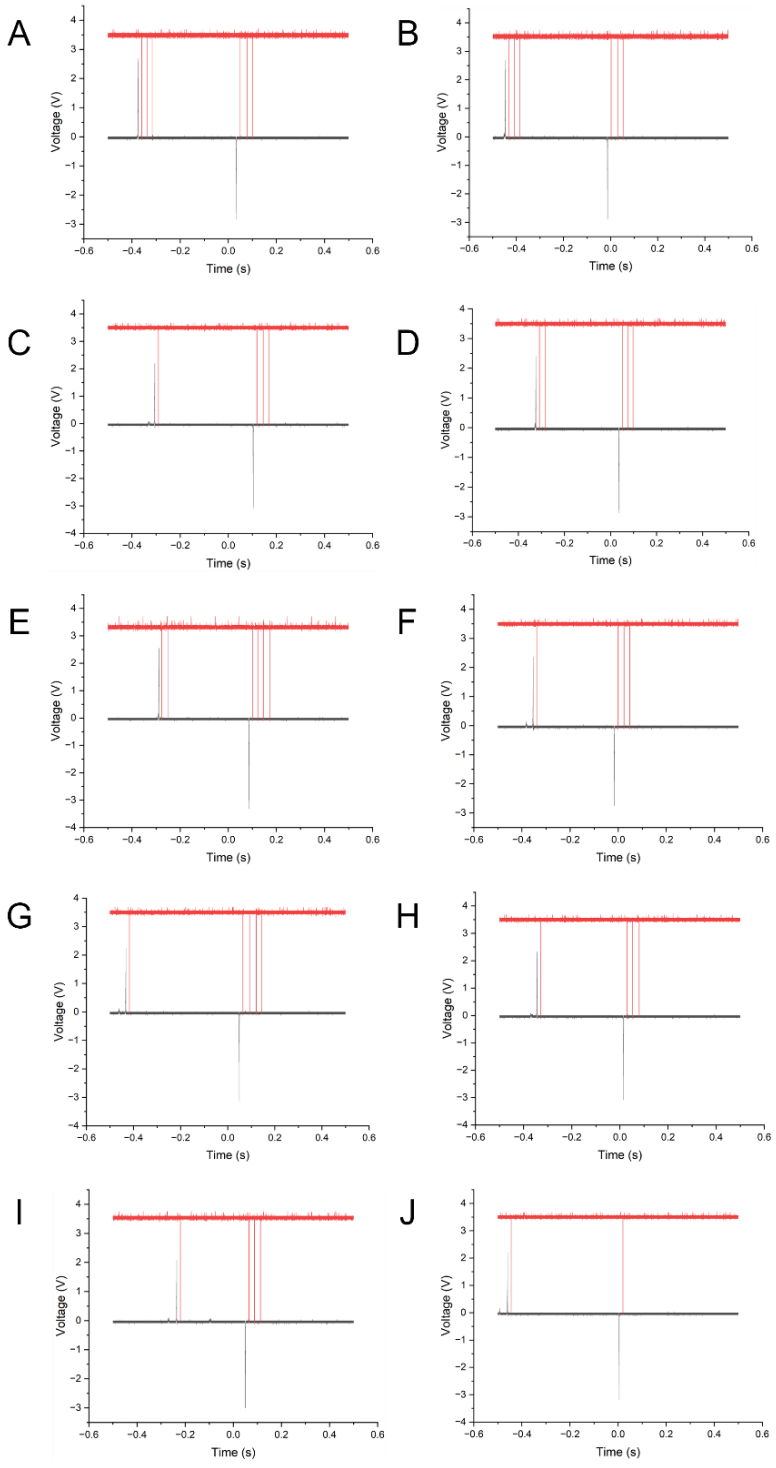

Fig. S17. Raw data for Figure 5C(ii).
The black curve represents the voltage output from the FMH (Fingertip Motion Harvester), while the red spikes overlaid on the curve indicate the Bluetooth Low Energy (BLE) signal detection events, as identified by the UART interface.

(A) group 1 test 1. (B) group 2 test 2. (C) group 3 test 3. (D) group 4 test 4. (E) group 5 test 5. (F) group 6 test 6. (G) group 7 test 7. (H) group 8 test 8. (I) group 9 test 9. (J) group 10 test 10.

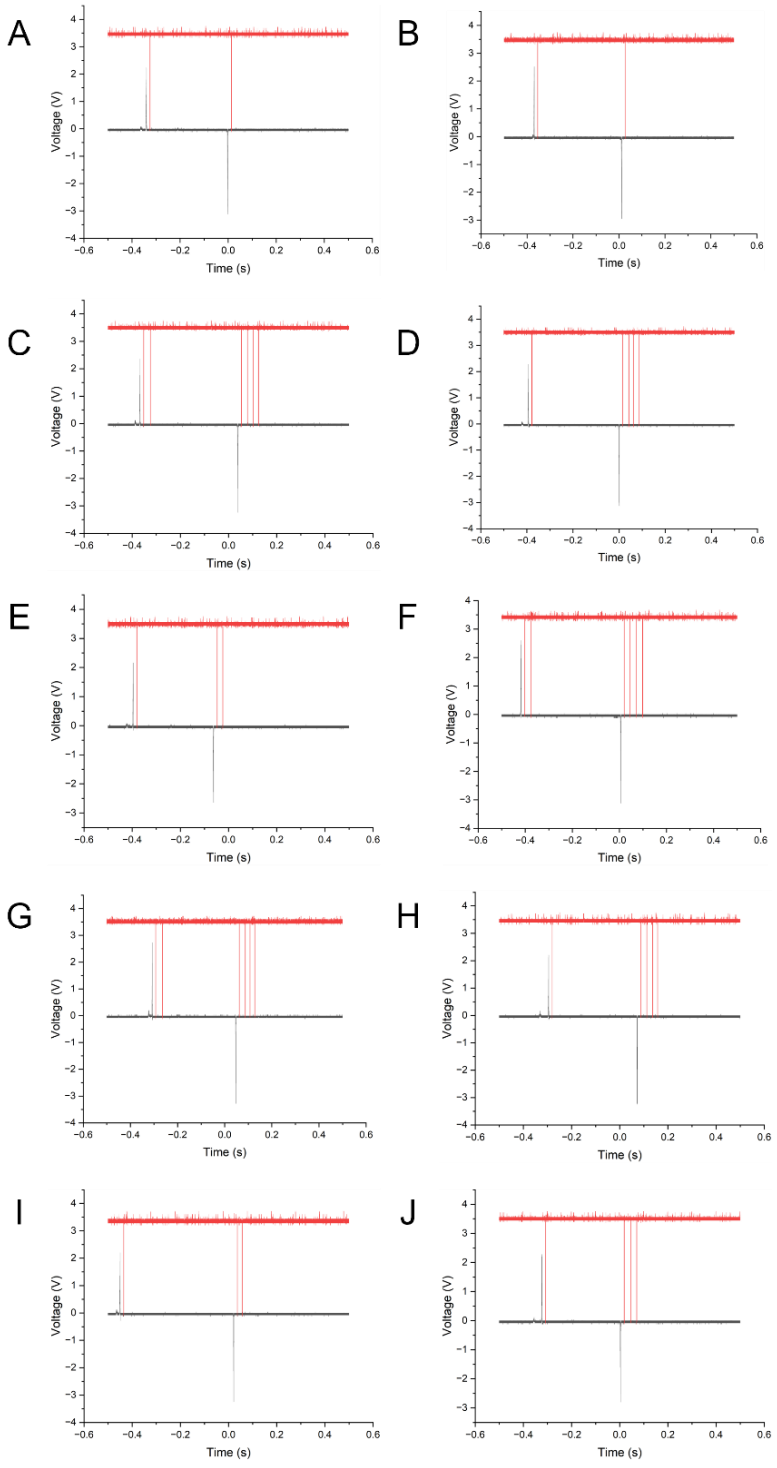

Fig. S18. Raw data for Figure 5C(iii).
The black curve represents the voltage output from the FMH (Fingertip Motion Harvester), while the red spikes overlaid on the curve indicate the Bluetooth Low Energy (BLE) signal detection events, as identified by the UART interface.

(A) group 1 test 1. (B) group 2 test 2. (C) group 3 test 3. (D) group 4 test 4. (E) group 5 test 5. (F) group 6 test 6. (G) group 7 test 7. (H) group 8 test 8. (I) group 9 test 9. (J) group 10 test 10.

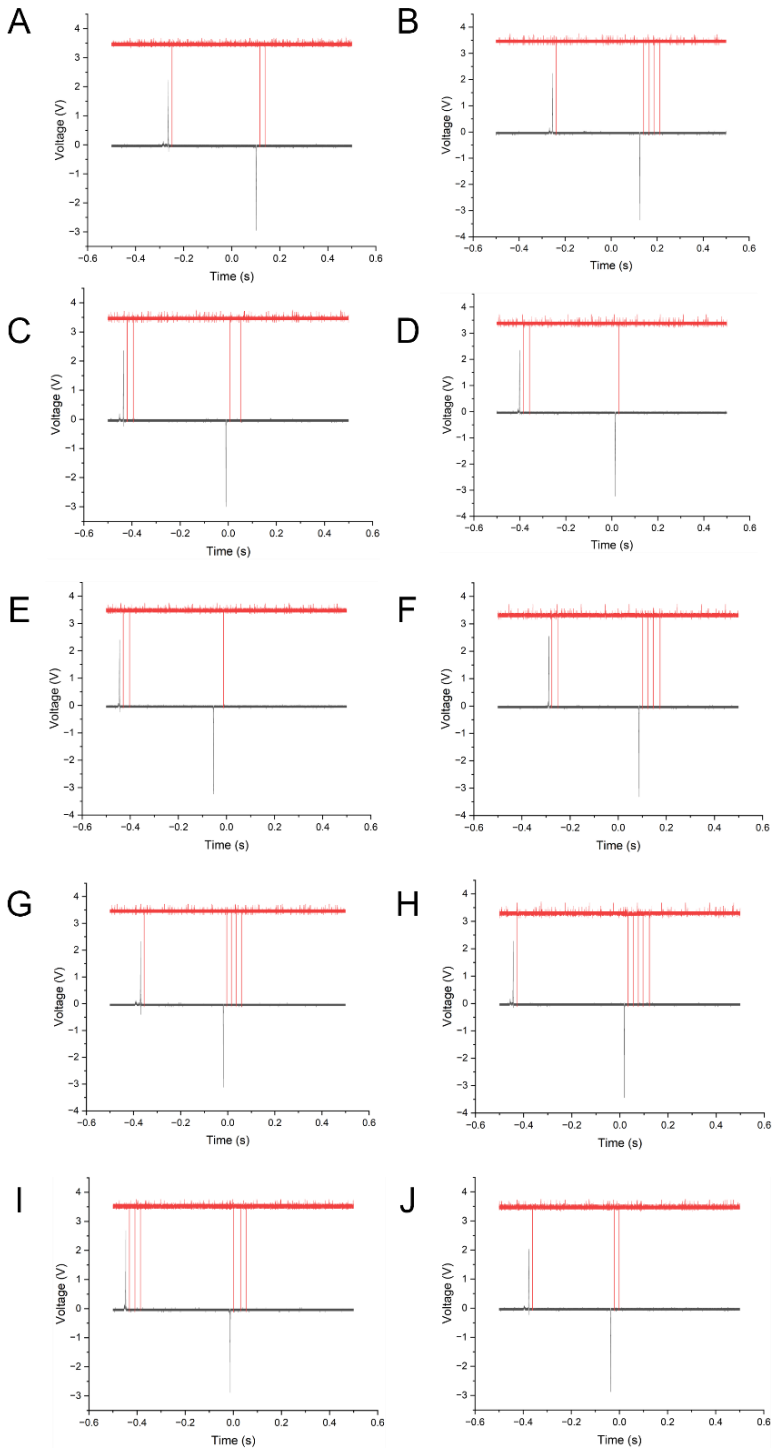

Fig. S19. Raw data for Figure 5C(iv).
The black curve represents the voltage output from the FMH (Fingertip Motion Harvester), while the red spikes overlaid on the curve indicate the Bluetooth Low Energy (BLE) signal detection events, as identified by the UART interface.

(A) group 1 test 1. (B) group 2 test 2. (C) group 3 test 3. (D) group 4 test 4. (E) group 5 test 5. (F) group 6 test 6. (G) group 7 test 7. (H) group 8 test 8. (I) group 9 test 9. (J) group 10 test 10.

Table S1. Static parameters used in analysis and evaluation.

Case		Parameters	Value
Case 1: Bistable case, soft buffering spring	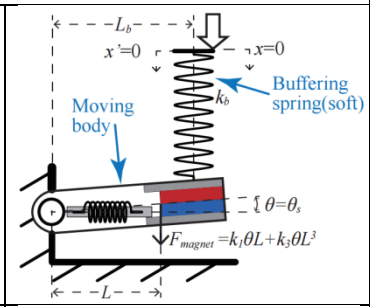	k_b	0.67 kN/m
Case 2: Bistable case, stiff buffering spring	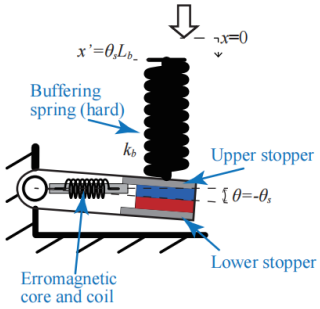	k_b	18.00 kN/m
Case 3: Monostable case	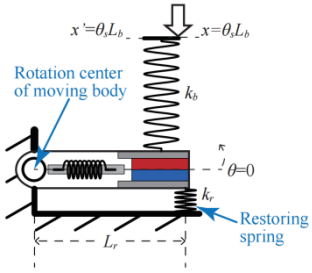	k_b	0.67 kN/m
		k_r	0.94 kN/m
Common parameters		L_b	16.93 mm
		L_r	18.91 mm
		L	13.10 mm
		k_1	-3.34 KN/m
		k_3	-25.27 GN/m^3
		k_s	1.00 MN/m
		J	0.60*10^{-6} kg*m^2
		θ_r	7.50°
		θ_s	1.91°
		c_s	0.20 kg*m^2/s

Table S2. Parameters of full-scale keyboard prototype.

Part	Parameters	Value
Single FMH in prototype	Size	23*20*53 mm^3
	Material of springs	Stainless steel
	Material of ferromagnetic core	Pure Iron
	Material of conductive stoppers	Silicon steel
	Material of other mechanical components	Resin (LEDO6060)
Full-scale keyboard	Size	30*13*7 cm^3
	Material of other mechanical components	Plastic(PLA)

Table S3. Summary of previously reported self-powered keyboard based on kinetic energy harvesting.

	Year	Harvesting Mode	Harvesting Power		Performance		Features	Applications	Ref.
			Peak Voltage	Output Power	Latency	Communication Range	Does it require additional power supply?		
1	2024	Electromagnetic energy harvesting	5V	140 mW	< 16 ms	16 m	No	Wireless keyboard demonstration;	This work
2	2015	Triboelectric energy harvesting	22 V	200 μW	N/A	N/A	Yes	LEDs; Supercapacitor charging demonstration; Wired keyboard demonstration based on additional ADC sampling;	[1]
3	2016	Triboelectric energy harvesting	30 V	16.7 μW	N/A	N/A	Yes	LEDs; Thermometer; Wired keyboard demonstration based on additional ADC sampling;	[2]
4	2018	Triboelectric energy harvesting	40 V	N/A	N/A	N/A	Yes	Wired keyboard demonstration based on additional ADC sampling;	[3]
5	2018	Triboelectric energy harvesting	13 V	N/A	N/A	N/A	Yes	Wired keyboard demonstration based on additional	[4]

								ADC sampling;	
6	2021	Triboelectric energy harvesting	2.5 V	N/A	N/A	N/A	Yes	LEDs; Wired keyboard demonstration based on additional ADC sampling;	[5]
7	2018	Triboelectric energy harvesting	1V	N/A	N/A	0.2 cm	No	Wireless keyboard demonstration;	[6]
8	2012	Piezoelectric energy harvesting	N/A	16.95 μW	N/A	N/A	No	LEDs;	[7]
9	2017	Piezoelectric energy harvesting	N/A	1.5 J/day	N/A	N/A	No	LEDs; Supercapacitor charging demonstration;	[8]
10	2021	Electromagnetic and triboelectric energy harvesting	120V	8.84mW	N/A	N/A	No	LEDs; Thermometer; Demonstration of Installing the Typewriter Key, Enter Key, and Space Key;	[9]

Table S4. Raw data for Figure 3H: average energy harvested from various participants. This test involved twenty participants, whose characteristics are detailed below.

Number	Characteristics	Maximum fingertip force (N)	Average harvested energy by an EMG (μJ)
1	Female, Short, Skinny	36.06	66.58948114
2	Female, Petite, Balanced	35.63	66.52060418
3	Female, Petite, Balanced	35.70	63.26683308
4	Female, Tallish, Balanced	32.60	62.59349732
5	Female, Tallish, Slim	33.10	63.85336140
6	Female, Tallish, Thin	32.33	60.86634300
7	Female, Tallish, Balanced	29.70	59.54269985
8	Female, Tall, Fit	30.54	61.40725164
9	Male, Petite, Slim	30.46	60.56876931
10	Male, Tallish, Chubby	34.95	62.70968058
11	Male, Tall, Thin	35.76	61.32465051
12	Male, Tall, Fit	35.19	61.31000980
13	Male, Petite, Balanced	22.85	56.86005214
14	Male, Tallish, Balanced	33.07	59.59019713
15	Male, Tall, Chubby	21.10	56.00441701
16	Female, Average, Balanced	16.50	47.95365594
17	Male, Average, Slim	21.00	52.07476446
18	Male, Average, Fit	16.70	49.71302555
19	Female, Tall, Slim	20.50	51.03403916
20	Male, Short, Slim	21.60	53.00484006

Table S5. Raw data for generating the error bar in Figure 3H: energy harvested from various participants. This test involved twenty participants, and each participant tested 10 times.

Participant Number	Test Number	Charging Voltage	Harvested energy (μJ)	Participant Number	Test Number	Charging Voltage	Harvested energy (μJ)
1	1	3.58	64.03428748	2	1	3.67	67.5060768
1	2	3.63	66.03461331	2	2	3.68	67.54528834
1	3	3.61	65.1171872	2	3	3.67	67.4766848
1	4	3.56	63.4819712	2	4	3.67	67.17333
1	5	3.75	70.2275132	2	5	3.68	67.76106328
1	6	3.64	66.26740262	2	6	3.53	62.36568992
1	7	3.69	67.9772192	2	7	3.57	63.54851357
1	8	3.69	68.00672	2	8	3.64	66.248
1	9	3.67	67.52566277	2	9	3.65	66.61735459
1	10	3.67	67.22223444	2	10	3.71	68.96404047
3	1	3.57	63.81496018	4	1	3.53	62.24334012
3	2	3.60	64.87681075	4	2	3.53	62.469354
3	3	3.59	64.51232	4	3	3.59	64.38784546
3	4	3.61	65.1749408	4	4	3.57	63.77688266
3	5	3.59	64.36872	4	5	3.52	62.10228944
3	6	3.53	62.39394698	4	6	3.53	62.4316448
3	7	3.58	64.24438414	4	7	3.51	61.57709052
3	8	3.56	63.20672794	4	8	3.53	62.2245006
3	9	3.29	54.0021248	4	9	3.53	62.4316448
3	10	3.64	66.0733952	4	10	3.53	62.2903808

Participant Number	Test Number	Charging Voltage	Harvested energy (µJ)	Participant Number	Test Number	Charging Voltage	Harvested energy (µJ)
5	1	3.58	63.94842828	6	1	3.45	59.37916327
5	2	3.61	65.0306048	6	2	3.50	61.11941468
5	3	3.52	61.7831552	6	3	3.49	60.87722392
5	4	3.56	63.50096448	6	4	3.49	60.79350873
5	5	3.58	64.15838415	6	5	3.51	61.66134332
5	6	3.56	63.37750556	6	6	3.50	61.3714051
5	7	3.60	64.66568168	6	7	3.47	60.09812213
5	8	3.50	61.3714051	6	8	3.52	61.98956409
5	9	3.62	65.66688	6	9	3.48	60.45922396
5	10	3.61	65.0306048	6	10	3.49	60.9144608
7	1	3.41	58.1814272	8	1	3.46	59.8856832
7	2	3.44	59.03048	8	2	3.48	60.4406912
7	3	3.47	60.3016992	8	3	3.50	61.0821152
7	4	3.48	60.50562048	8	4	3.50	61.3714051
7	5	3.45	59.54469285	8	5	3.50	61.0821152
7	6	3.49	60.8586272	8	6	3.51	61.4742048
7	7	3.45	59.39756704	8	7	3.50	61.14738801
7	8	3.45	59.34243317	8	8	3.54	62.5353283
7	9	3.45	59.59992058	8	9	3.55	62.9983008
7	10	3.43	58.6645308	8	10	3.52	62.05528461

Participant Number	Test Number	Charging Voltage	Harvested energy (µJ)	Participant Number	Test Number	Charging Voltage	Harvested energy (µJ)
9	1	3.42	58.34528	10	1	3.51	61.7269248
9	2	3.49	61.07278337	10	2	3.48	60.42216128
9	3	3.48	60.58913729	10	3	3.53	62.37512
9	4	3.45	59.46189926	10	4	3.55	63.03618072
9	5	3.52	62.04591396	10	5	3.54	62.5447712
9	6	3.36	56.46591022	10	6	3.57	63.69119625
9	7	3.52	61.88629903	10	7	3.59	64.521911
9	8	3.53	62.37512	10	8	3.58	64.18704441
9	9	3.50	61.39943604	10	9	3.54	62.70519708
9	10	3.52	62.04591396	10	10	3.52	61.88629903
11	1	3.52	61.88629903	12	1	3.44	59.14505742
11	2	3.53	62.37512	12	2	3.53	62.18690064
11	3	3.49	60.9144608	12	3	3.51	61.49759471
11	4	3.55	62.86586391	12	4	3.49	60.80745726
11	5	3.50	61.39943604	12	5	3.51	61.65200246
11	6	3.54	62.5447712	12	6	3.49	60.7330952
11	7	3.50	61.39943604	12	7	3.54	62.72882
11	8	3.50	61.39943604	12	8	3.48	60.50562048
11	9	3.48	60.58913729	12	9	3.50	61.11472977
11	10	3.40	57.87254475	12	10	3.54	62.72882

Participant Number	Test Number	Charging Voltage	Harvested energy (µJ)	Participant Number	Test Number	Charging Voltage	Harvested energy (µJ)
13	1	3.32	55.06775328	14	1	3.30	54.43241242
13	2	3.30	54.6085152	14	2	3.51	61.49759471
13	3	3.35	56.1527072	14	3	3.53	62.42221044
13	4	3.37	56.61837957	14	4	3.45	59.5953288
13	5	3.38	57.24824508	14	5	3.45	59.66899124
13	6	3.39	57.40176632	14	6	3.50	61.11472977
13	7	3.40	57.7184288	14	7	3.50	61.4181152
13	8	3.40	57.7184288	14	8	3.34	55.8849312
13	9	3.43	58.6645308	14	9	3.34	55.7379272
13	10	3.39	57.40176632	14	10	3.58	64.12973028
15	1	3.22	51.71328	16	1	3.12	48.516125
15	2	3.13	49.10978	16	2	3.15	49.6125
15	3	3.28	53.890445	16	3	3.15	49.6125
15	4	3.18	50.530205	16	4	3.08	47.524445
15	5	3.25	52.780005	16	5	3.08	47.524445
15	6	3.20	51.2	16	6	3.08	47.524445
15	7	3.05	46.543005	16	7	3.13	49.10978
15	8	3.20	51.07208	16	8	3.17	50.2445
15	9	3.20	51.07208	16	9	3.17	50.2445
15	10	3.28	53.890445	16	10	3.25	52.910045

Participant Number	Test Number	Charging Voltage	Harvested energy (µJ)	Participant Number	Test Number	Charging Voltage	Harvested energy (µJ)
17	1	3.23	52.1645	18	1	3.15	49.6125
17	2	3.27	53.4645	18	2	3.14	49.298
17	3	3.20	51.2	18	3	3.18	50.562
17	4	3.25	52.8125	18	4	3.07	47.1245
17	5	3.24	52.488	18	5	3.19	50.8805
17	6	3.12	48.672	18	6	3.16	49.928
17	7	3.21	51.5205	18	7	3.21	51.5205
17	8	3.20	51.2	18	8	3.18	50.562
17	9	3.27	53.4645	18	9	3.04	46.208
17	10	3.24	52.488	18	10	3.09	47.7405
19	1	3.20	51.2	20	1	3.18	50.562
19	2	3.03	45.9045	20	2	3.07	47.1245
19	3	2.92	42.632	20	3	3.19	50.8805
19	4	2.78	38.642	20	4	3.16	49.928
19	5	2.92	42.632	20	5	3.21	51.5205
19	6	2.93	42.9245	20	6	3.18	50.562
19	7	2.99	44.7005	20	7	3.04	46.208
19	8	2.95	43.5125	20	8	3.09	47.7405
19	9	3.02	45.602	20	9	3.20	51.2
19	10	2.85	40.6125	20	10	3.03	45.9045

Movie S1. Demonstration of the power generation of an individual key button.

The oscilloscope in the video records the voltage output.

Movie S2. Demonstration of the functionality of an individual key button.

The oscilloscope in the video records the voltage output and the TX signal voltage at the receiver end. The computer displays the message received by the serial port software.

Movie S3. Demonstration of the operation of the assembled keyboard.

Movie S4. Demonstration of the open-circuit output voltage of a single key button.

References

1. J. Chen, G. Zhu, J. Yang, Q. Jing, P. Bai, W. Yang, X. Qi, Y. Su, Z. L. Wang, Personalized keystroke dynamics for self-powered human-machine interfacing, ACS nano 9 (1) (2015) 105–116.
2. S. Li, W. Peng, J. Wang, L. Lin, Y. Zi, G. Zhang, Z. L. Wang, All-elastomer-based triboelectric nanogenerator as a keyboard cover to harvest typing energy, ACS Nano 10 (8) (2016) 7973–7981.
3. C. Wu, W. Ding, R. Liu, J. Wang, A. C. Wang, J. Wang, S. Li, Y. Zi, Z. L. Wang, Keystroke dynamics enabled authentication and identification using triboelectric nanogenerator array, Materials Today 21 (3) (2018) 216 – 222.
4. S.-B. Jeon, S.-J. Park, W.-G. Kim, I.-W. Tcho, I.-K. Jin, J.-K. Han, D. Kim, Y.-K. Choi, Self-powered wearable keyboard with fabric based triboelectric nanogenerator, Nano energy 53 (2018) 596-603.
5. J. Yi, K. Dong, S. Shen, Y. Jiang, X. Peng, C. Ye, Z. L. Wang, Fully fabric-based triboelectric nanogenerators as self-powered human-machine interactive keyboards, Nano-micro letters 13 (2021) 1-13.
6. W. Yin, Y. Xie, J. Long, P. Zhao, J. Chen, J. Luo, X. Wang, S. Dong, A self-power-transmission and non-contact-reception keyboard based on a novel resonant triboelectric nanogenerator (r-teng), Nano Energy 50 (2018) 16 – 24.
7. L. Beker, A. Muhtaroglu, H. Külah, A novel method for piezoelectric energy harvesting from keyboard, in: Active and Passive Smart Structures and Integrated Systems 2012, Vol. 8341, SPIE, 2012, pp.729 – 736.
8. T. Page, A feasibility study in energy harvesting from piezoelectric keyboards, International Journal of Energy Optimization and Engineering (IJEOE) 6 (2) (2017) 1 – 23.
9. P. Maharjan, T. Bhatta, C. Park, H. Cho, K. Shrestha, S. Lee, M. Salauddin, M. Rahman, S. S. Rana, J. Y. Park, High-performance keyboard typing motion driven hybrid nanogenerator, Nano Energy 88 (2021) 106232.